Kinetic Studies on the Reactions of Heptafluoropropanes with O(^{3}P) and H Atoms at High Temperatures

Osami Yamamoto, Kazuo Takahashi,* and Tadaaki Inomata

Department of Chemistry, Sophia University, 7-1 Kioi-cho, Chiyoda-ku, Tokyo 102-8554, Japan

Received: September 7, 2003; In Final Form: December 25, 2003

The reactions of 2*H*-heptafluoropropane (CF_3CHFCF_3, HFC-227ea) with O(^{3}P) and H atoms have been studied at high temperatures by using a shock tube technique coupled with atomic resonance absorption spectroscopy. Electronically ground-state oxygen and hydrogen atoms were produced by the laser photolysis of sulfur dioxide and the thermal decomposition of ethyl iodide, respectively. The rate coefficients for the reactions $CF_3CHFCF_3 + O(^3P) \rightarrow i\text{-}C_3F_7 + OH$ (1a) and $CF_3CHFCF_3 + H \rightarrow i\text{-}C_3F_7 + H_2$ (2a) were experimentally determined from the decay of O(^{3}P) and H atoms as $k_{1a} = 10^{-10.27\pm0.67}$ exp[−(56 ± 13) kJ mol^{-1}/*RT*] cm^3 molecule^{-1} s^{-1} (880−1180 K) and $k_{2a} = 10^{-9.15\pm0.66}$ exp[−(63 ± 14) kJ mol^{-1}/*RT*] cm^3 molecule^{-1} s^{-1} (1000−1180 K). These results showed that reaction 2a was faster than reaction 1a by a factor of 7−8 over the present experimental temperature range. Both rate coefficients were much smaller than the previous kinetic data for the reactions of propane with O(^{3}P) and H atoms, because of an electron-attracting effect of fluorine atoms. To compare the reactivities between isomers, the rate coefficients for the reactions of 1*H*-heptafluoropropane, $CHF_2CF_2CF_3 + O(^3P) \rightarrow n\text{-}C_3F_7 + OH$ (3a) and $CHF_2CF_2CF_3 + H \rightarrow n\text{-}C_3F_7 + H_2$ (4a), were also determined by using the same technique as $k_{3a} = 10^{-10.13\pm0.52}$ exp[−(55 ± 10) kJ mol^{-1}/*RT*] cm^3 molecule^{-1} s^{-1} (880−1180 K) and $k_{4a} = 10^{-9.44\pm0.32}$ exp[−(57 ± 7) kJ mol^{-1}/*RT*] cm^3 molecule^{-1} s^{-1} (1000−1180 K). Furthermore, the rate coefficients for reactions 1a and 2a were calculated with the transition-state theory (TST). Structural parameters and vibrational frequencies of the reactants and the transition states required for the TST calculation were obtained from the MP2(full)/6-31G(d) ab initio molecular orbital (MO) calculation. The energy barrier, $E_0^{\ddagger}$, was adjusted until the TST rate coefficient most closely matched the observed one. The fitting results of $E_0^{\ddagger}$(1a) = 51 kJ mol^{-1} and $E_0^{\ddagger}$(2a) = 41 kJ mol^{-1} were in agreement with the G2(MP2) energy barriers, within the expected uncertainty.

Introduction

Halons, bromine-containing perhalogenated carbon compounds such as CF_3Br, CF_2BrCl, and $C_2F_4Br_2$, have been used for many years as gaseous fire-extinguishing agents.[1] They have high fire-extinguishing abilities because of their chemical suppression mechanism; that is, bromine-containing species can catalytically remove active species from the combustion zone.[2−4] Due to serious concerns about ozone depletion in the stratosphere,[5] however, the production of halons has been prohibited and intensive research programs have been undertaken to find effective replacements. Around 10 years ago, hydrofluorocarbons and perfluorocarbons were proposed as one of the candidates to replace halons. Some of them, such as HFC-23 (CHF_3), HFC-227ea (CF_3CHFCF_3), and FC-3−1−10 (C_4F_{10}), have already been commercialized.

The construction of the reaction mechanism for fluorocarbons is needed not only to understand their chemical roles in a flame but also to find other fluorocarbons that have higher fire-extinguishing abilities. Under these circumstances, a research group of the National Institute of Standards and Technology in the U.S.A.[6] has constructed the detailed reaction mechanism for C1 and C2 fluorocarbons, so that the modeling of the CHF_3-inhibited flames became possible. The reaction mechanisms for fluorocarbons higher than C2 have also been reported by some groups[7,8] but cannot be accepted as comprehensively reliable schemes, because most of the kinetic data for the elementary reactions involving C3 and C4 fluorocarbons are estimated from those for the analogous reactions of C2 fluorocarbons or fluorine-free hydrocarbons.

Since some years ago, we have performed kinetic studies on key reactions for the HFC-23 combustion and were successful in obtaining some important results.[9−11] As the next, new research project, we are interested in the kinetics of the elementary reactions for HFC-227ea combustion. Recently, Hynes et al.[12] have experimentally determined the rate coefficients for the following reactions:

$$CF_3CHFCF_3 + F \rightarrow i\text{-}C_3F_7 + HF \quad (6)$$

$$CF_3CHFCF_3 \rightarrow CF_3CHF + CF_3 \quad (7a)$$

$$CF_3CHFCF_3 \rightarrow C_3F_6 + HF \quad (7b)$$

But there are no previous works for the other reactions involving CF_3CHFCF_3. In the present study, we focused on the bimolecular reactions of CF_3CHFCF_3 with O(^{3}P) and H atoms, which are among the most important chain carriers in combustion reactions. These rate coefficients were directly measured at high temperatures by using a shock tube technique coupled with atomic resonance absorption spectroscopy (ARAS). To compare the reactivities between isomers, the kinetics of the reactions of $CHF_2CF_2CF_3$ with O(^{3}P) and H atoms was also studied.

* Corresponding author. Phone: +81-3-3238-3457. Fax: +81-3-3238-3478. E-mail: takaha-k@sophia.ac.jp.

10.1021/jp036669k CCC: $27.50
Published on Web 01/31/2004

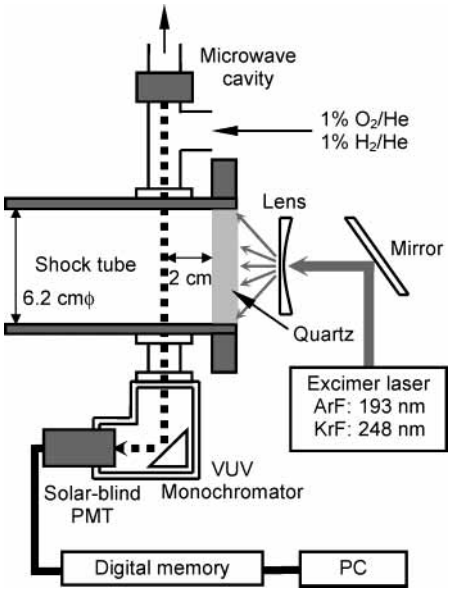

Figure 1. Schematic apparatus for O(^{3}P) and H atom detections and laser photolysis arranged at the end of the shock tube.

Furthermore, these rate coefficients were calculated with the transition-state theory (TST). The validity of the experimental results is discussed.

Experimental Section

Shock Tube. All experiments were performed behind reflected shock waves in a diaphragmless stainless steel shock tube, which consists of a 5.84-*l* driver section and a 4.6 m long test section with 6.23 cm i.d. Details of the structure and the performance have been described previously.[9] The test section was evacuated by a turbomolecular pump to pressures down to 1×10^{-4} Pa, in which the residual gas was practically free from hydrocarbons. To measure incident shock velocity, three piezoelectric pressure transducers were mounted on the shock tube walls at 25 cm intervals from the end of the test section. The temperature and pressure of the shock-heated test gas were calculated from the incident shock velocity using the conventional method. Driver gases were prepared by mixing helium, nitrogen, and carbon dioxide, depending on requested temperatures.

Optical System for Atom Detection and Calibration. The time-resolved concentrations of electronically ground-state O ($2p^4\ ^3P_J$) and H ($1s\ ^2S_0$) atoms were monitored by ARAS. Figure 1 shows a schematic apparatus for ARAS and laser photolysis arranged near the end of the test section. A microwave discharge lamp, in which helium containing 1% oxygen or hydrogen was flowing at a pressure of 4×10^2 Pa, was used as a light source. The wavelengths of monitored resonance light were 130.2, 130.4, and 130.6 nm ($3s\ ^3S_1{}^0 \leftarrow 2p^4\ ^3P_J$) for O(^{3}P) atoms and 121.6 nm ($2p\ ^2P_{1/2} \leftarrow 1s\ ^2S_0$) for H atoms. The resonance radiation from the lamp passed through two MgF_2 windows (1 mm thickness) mounted on the shock tube walls at a position 2 cm from the end. The transmitted light was isolated by a 20 cm VUV monochromator (Minutesman 302-VM), which was evacuated to a pressure less than 5×10^{-3} Pa and detected by a solar-blind photomultiplier tube (Hamamatsu Photonics R1459). The signal was then recorded by a digital storage oscilloscope (Hitachi VC-6165).

Calibration experiments were performed behind reflected shock waves in 0.5−64 ppm N_2O/Ar mixtures for the O atom ARAS and in 0.5−2 ppm C_2H_5I/Ar mixtures for the H atom ARAS. Details of the principles and procedures have been described elsewhere.[9,10] The calibration results could not follow the Lambert−Beer law, due to self-absorption or self-reversal. So we assumed the modified Lambert−Beer equation:

$$1 - \frac{I}{I_0} = 1 - \exp\{-\sigma_0 T^\beta l [\mathrm{X}]^\gamma\}$$

where l means the optical path length (=6.23 cm). The following three parameters σ_0, β, and γ were determined for both atoms by least-squares methods and were used to convert from absorptions to absolute concentrations:

$$\sigma_0(\mathrm{O}) = 10^{-10.57\pm0.55}\ \mathrm{cm}^{3\gamma-1}\mathrm{K}^{-\beta} \qquad \beta(\mathrm{O}) = 0$$
$$\gamma(\mathrm{O}) = 0.714 \pm 0.041 \qquad \text{at } 130.2-6 \text{ nm}$$
$$\sigma_0(\mathrm{H}) = 10^{-13.06\pm1.31}\ \mathrm{cm}^{3\gamma-1}\mathrm{K}^{-\beta} \qquad \beta(\mathrm{H}) = 1.46 \pm 0.40$$
$$\gamma(\mathrm{H}) = 0.650 \pm 0.031 \qquad \text{at } 121.6 \text{ nm}$$

Laser Equipment for Photolysis. ArF and KrF excimer lasers (LAMBDA PHYSIK COMPex 102), of which wavelengths were 193 and 248 nm, respectively, were applied for the photolysis. The laser beam was ignited with a 100 μs delay after the arrival of a reflected shock wave and was introduced to the ARAS optical path through a 1 cm thick quartz endplate of the shock tube, as shown in Figure 1. The beam size was 38×8 mm^2 at the observation station and the intensities were 3.6×10^{16} photons cm^{-2} for the ArF laser and 1.2×10^{17} photons cm^{-2} for the KrF laser.

Measurements and Gases. Measurements of the rate coefficient for the reaction $CF_3CHFCF_3 + O(^3P)$ were carried out in mixtures of CF_3CHFCF_3, SO_2, and Ar by detecting O(^{3}P) atoms. Triplet electronic state oxygen atoms were generated by the laser photolysis of SO_2. On the other hand, the rate coefficient for the reaction $CF_3CHFCF_3 + H$ were obtained from the decay of H atoms in mixtures of CF_3CHFCF_3, C_2H_5I, and Ar. Hydrogen atoms were yielded through the thermal decomposition of C_2H_5I. The experimental temperature ranges were 880−1180 K for the O(^{3}P) atom reaction and 1000−1180 K for the H atom reaction, respectively, and the total density was fixed at 6.0×10^{18} molecules cm^{-3} in all experiments. To compare with these results, we also studied the reactions of $CHF_2CF_2CF_3$ with O(^{3}P) and H atoms under the same experimental conditions.

1*H*- and 2*H*-heptafluoropropanes used in the present experiments were produced by SynQuest Labs.; their purities were >97% and >98%. Ethyl iodide (Aldrich; >99%) was purified with trap-to-trap distillation, and research grade sulfur dioxide (Takachiho; >99.9%) was used as delivered. These agents were diluted in scientific grade argon (Nippon Sanso; >99.9999%).

Results and Discussion

Reaction of CF_3CHFCF_3 with O(^{3}P). For the reaction of CF_3CHFCF_3 with O(^{3}P), the following three abstraction channels are possible:

$$CF_3CHFCF_3 + O(^3P) \rightarrow i\text{-}C_3F_7 + OH \qquad (1a)$$

$$CF_3CHFCF_3 + O(^3P) \rightarrow i\text{-}C_3HF_6 + OF \qquad (1b)$$

$$CF_3CHFCF_3 + O(^3P) \rightarrow n\text{-}C_3HF_6 + OF \qquad (1c)$$

To examine which is the main channel, an ab initio MO calculation was performed by using the Gaussian 98 program.[13]

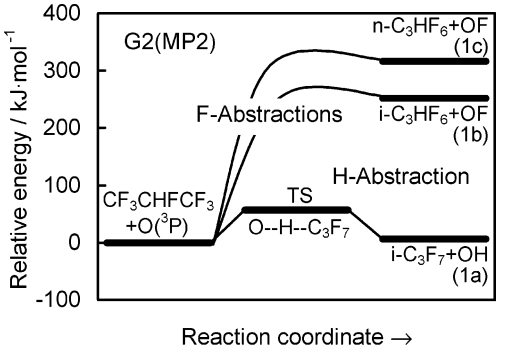

Figure 2. Energy diagram for the reaction $CF_3CHFCF_3 + O(^3P)$. The energies are calculated at the G2(MP2) level and are corrected for the zero-point vibrations.

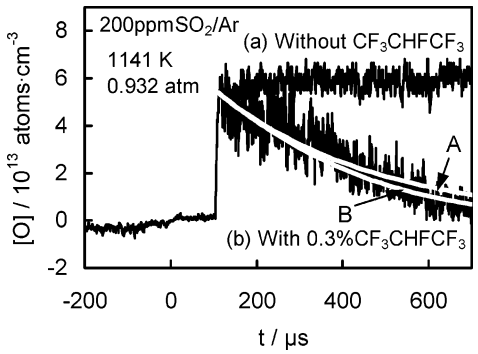

Figure 3. Typical concentration profiles of $O(^3P)$ atoms in (a) 200 $ppmSO_2/Ar$ and (b) 0.3% $CF_3CHFCF_3/200$ $ppmSO_2/Ar$ mixtures. Two white lines denote profiles calculated on the basis of (A) only reaction 1a and (B) scheme I shown in Table 1, which consists of reaction 1a and 10 other side reactions.

Figure 2 shows the energy diagram calculated at the G2(MP2) level.[14] The calculation results show that the most energetically favorable channel is the H abstraction 1a by an $O(^3P)$ atom and that the F abstraction channels 1b and 1c are negligible due to their high energy barriers, over 250 kJ mol^{-1}. Therefore, the main product channel can be concluded to be reaction 1a.

Measurements of the rate coefficient for reaction 1a were carried out in mixtures of 0.1−0.5% CF_3CHFCF_3 and 200−400 ppm SO_2 diluted in argon. A typical concentration profile of $O(^3P)$ atoms is shown in Figure 3, together with a profile in the mixture that did not contain CF_3CHFCF_3. Time zero in the figure denotes the arrival of a reflected shock wave at the observation station. Due to the relatively high concentrations of the reactants, the molecular absorptions of CF_3CHFCF_3 and SO_2 were found to be around 30 and 20%, respectively. So the net absorption obtained by subtracting these molecular absorptions from the original ARAS signal was converted to the absolute concentration of $O(^3P)$ atoms. In the SO_2/Ar mixture, the number of $O(^3P)$ atoms rapidly rises due to the photolysis of SO_2 induced by irradiation of the ArF excimer laser at $t \approx 100$ μs, which is $SO_2 + h\nu \rightarrow SO + O(^3P)$ (14), and later the concentration of $O(^3P)$ atoms takes a constant value. In the presence of CF_3CHFCF_3, $O(^3P)$ atoms decay gradually through reaction 1a after a rapid formation by the photolysis. The more remarkable decay of $O(^3P)$ atoms is favorable for the kinetic analysis, but such experimental conditions could not be established. If the initial concentration of CF_3CHFCF_3 was higher to enhance reaction 1a, the molecular absorption of CF_3CHFCF_3 was increased with the initial concentration, leading to deterioration of the signal-to-noise ratio for the measured profiles. The absorption of unknown species, which is probably caused by vibrationally excited products of the CF_3CHFCF_3 thermal decomposition, was observed at temperatures higher than 1180 K. So the upper limit of the experimental temperatures was set to be 1180 K.

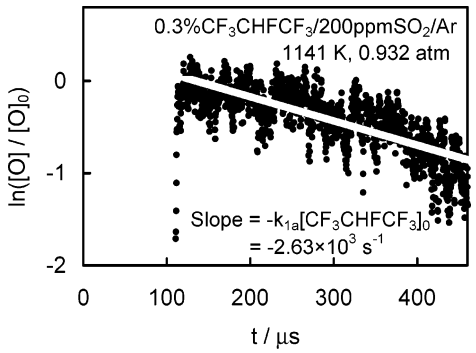

Figure 4. Typical plot of logarithmical concentration of $O(^3P)$ atoms as a function of reaction time in 0.3% $CF_3CHFCF_3/200$ $ppmSO_2/Ar$ mixture.

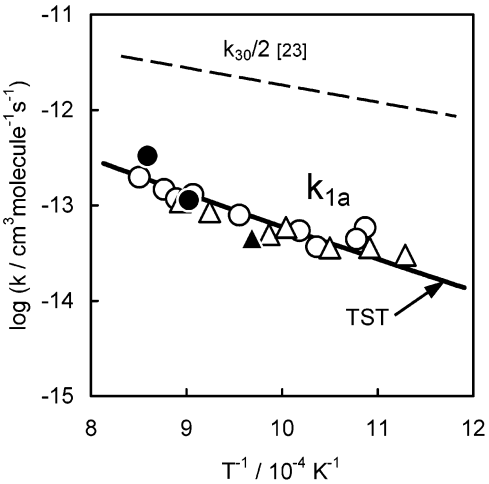

Figure 5. Arrhenius plot of the rate coefficient for reaction 1a: (○) 0.3% $CF_3CHFCF_3/200$ $ppmSO_2/Ar$, ArF-LP; (△) 0.5% $CF_3CHFCF_3/200$ $ppmSO_2/Ar$, ArF-LP; (●) 0.1% $CF_3CHFCF_3/400$ $ppmSO_2/Ar$, KrF-LP; (▲) 0.3% $CF_3CHFCF_3/400$ $ppmSO_2/Ar$, KrF-LP. The broken line denotes half of the rate coefficient for the reaction $C_3H_8 + O(^3P) \rightarrow i\text{-}C_3H_7 + OH$ (30).[23] The solid line shows the TST result calculated with $E_0^{\ddagger}(1a) = 51$ kJ mol^{-1}.

In the present conditions, the concentration of $O(^3P)$ atoms generated by the photolysis is only a few ppm. This means the following pseudo-first-order rate equation can be applied in this system if any secondary reactions are negligible:

$$\ln [O] = -k_{1a}[CF_3CHFCF_3]_0\, t + C$$

where t is the reaction time and k_{1a} is the second-order rate coefficient for reaction 1a. An integration constant is expressed with C. Figure 4 shows that a linear relationship exists between the logarithm of [O] and t. In all experiments, the straight line was drawn until the time when $O(^3P)$ atoms concentration was decreased to 63% of the initial concentration. From the slope of this straight line, k_{1a} was determined. An Arrhenius plot of k_{1a} obtained in this method is shown in Figure 5. These numerical data are summarized in the Supporting Information, together with the detailed experimental conditions. The measured values of k_{1a} were found to be independent of the initial concentration of CF_3CHFCF_3, which is an indirect piece of evidence that secondary reactions give no serious error in the determination of k_{1a}. A KrF (248 nm) laser was also used instead

TABLE 1: Reaction Schemes for (I) CF_3CHFCF_3/SO_2 and (II) CF_3CHFCF_3/C_2H_5I Systems

				forward rate coefficient[b]			
no.	reaction	scheme[a]		log A	n	E_a/R	ref
1a	$CF_3CHFCF_3 + O(^3P) \rightarrow CF_3CFCF_3 + OH$	I		−10.27	0.00	6740	c
2a	$CF_3CHFCF_3 + H \rightarrow CF_3CFCF_3 + H_2$	II			adjusted		
5	$CF_3CHFCF_3 + OH \rightarrow CF_3CFCF_3 + H_2O$	I		−11.78	0.00	2010	8
7a	$CF_3CHFCF_3 \rightarrow CF_3CHF + CF_3$	I & II		15.90	0.00	42800	12
7b	$CF_3CHFCF_3 \rightarrow C_3F_6 + HF$	I & II		12.90	0.00	35000	12
8	$CF_3CFCF_3 + O(^3P) \rightarrow CF_3CFO + CF_3$	I		−10.40	0.00	0	8
9	$CF_3CFCF_3 + H \rightarrow C_3F_6 + HF$	II		39.60	−13.90	22500	8
10	$CF_3CFCF_3 + OH \rightarrow CF_3CO + CF_3 + HF$	I		−10.44	0.00	0	8
11	$CF_3CFCF_3 \rightarrow CF_3CF + CF_3$	I & II		14.00	0.00	38200	8
12	$CF_3 + O(^3P) \rightarrow CF_2O + F$	I		−10.59	0.00	0	10
13	$CF_3 + H \rightarrow CF_2 + HF$	II		−10.05	0.00	0	10
15	$SO_2 + M = SO + O(^3P) + M$[d]	I		−7.33	0.00	58600	17
16	$SO_2 + O(^3P) = SO + O_2$[d]	I		−11.08	0.00	9800	18
17	$O(^3P) + O(^3P) + M = O_2 + M$[d]	I		−34.28	0.00	−900	19
18a	$C_2H_5I = C_2H_5 + I$[d]	II			adjusted		
18b	$C_2H_5I = C_2H_4 + HI$[d]	II		11.11	0.00	19500	20
19	$H + C_2H_4(+M) = C_2H_5(+M)$[d,e]	II	high	−10.44	0.00	1030	21
			low	−19.76	−2.80	−24	21
20	$C_2H_5I + H = C_2H_5 + HI$[d]	II		−9.24	0.00	1760	22
21	$C_2H_5I + I = C_2H_5 + I_2$[d]	II		−10.18	0.00	8410	22
22	$F + F + M = F_2 + M$[d]	II		−33.56	0.00	0	22
23	$F + H + M = HF + M$[d]	II		−29.58	−1.00	0	22
24	$F_2 + H = HF + F$[d]	II		−9.70	0.00	1210	22
25	$HF + H = H_2 + F$[d]	II		−9.44	0.00	17000	22
26	$I + I + M = I_2 + M$[d]	II		−34.57	1.00	0	22
27	$I + H + M = HI + M$[d]	II		−34.48	1.00	0	22
28	$I_2 + H = HI + I$[d]	II		−9.39	0.00	0	22
29	$HI + H = H_2 + I$[d]	II		−10.26	0.00	0	22

[a] Schemes I and II mean the kinetic models used in the CF_3CHFCF_3/SO_2 and CF_3CHFCF_3/C_2H_5I systems, respectively. [b] Forward rate coefficients in the form $k=AT^n\exp(-E_a/RT)$, in cm^3, molecule, and s units. [c] Determined in this work. [d] Reverse rate coefficients were calculated from the forward ones and the equilibrium constants. [e] Pressure-dependent falloff reaction. At any pressure, the rate coefficient was calculated from $k=k_\infty[(k_0[M]/k_\infty)/(1 + k_0[M]/k_\infty)]$ where k_0 and k_∞ are low- and high-pressure limit rate coefficients.

of ArF (193 nm), resulting in the same value of k_{1a}. This result confirms that laser light has little effect on species other than SO_2, e.g., fluorocarbons. A least-squares fit of the data yielded the following Arrhenius expression over the temperature range of 880 to 1180 K:

$$k_{1a} = 10^{-10.27\pm0.67} \times \exp[-(56 \pm 13)\ \text{kJ mol}^{-1}/RT]\ \text{cm}^3\ \text{molecule}^{-1}\ \text{s}^{-1}$$

where all error limits expressed in the present paper mean two standard deviations.

To check the influence of secondary reactions more strictly, a numerical calculation was performed by using the Sandia CHEMKIN-II[15] and SENKIN[16] program codes. The detailed reaction model is summarized in scheme I of Table 1: it consists of reaction 1a and 10 other side reactions. The Arrhenius expression of k_{1a} determined under the pseudo-first-order approximation was used in the calculation. An example of the numerical results is shown with line B in Figure 3, and line A means the concentration profile calculated on the basis of only reaction 1a. A slight difference between lines A and B is found in the reaction time later than 400 μs; line B reproduces the observed profile better than line A. In the detailed reaction model, i-C_3F_7 radicals formed through the focus reaction 1a react with $O(^3P)$ atoms. Subsequently, the product CF_3 radicals also consume $O(^3P)$ atoms.

$$i\text{-}C_3F_7 + O(^3P) \rightarrow CF_3CFO + CF_3 \quad (8)$$

$$CF_3 + O(^3P) \rightarrow CF_2O + F \quad (12)$$

At temperatures higher than 1050 K, the thermal decomposition of i-C_3F_7 begins to occur and to affect the consumption of $O(^3P)$ atoms.

$$i\text{-}C_3F_7 \rightarrow CF_3CF + CF_3 \quad (11)$$

However, the contribution of these secondary reactions appears only after a large number of i-C_3F_7 are produced through reaction 1a. The pseudo-first-order approximation can be applied until a reaction extent of 50%, so that no secondary reactions are concluded to affect the determination of k_{1a} in the present work.

The kinetic data for reaction 1a have not previously been reported at any temperatures. To discuss the validity of the present result, the measured values of k_{1a} are compared with the kinetic data for the reaction of fluorine-free propane with $O(^3P)$.

$$C_3H_8 + O(^3P) \rightarrow i\text{-}C_3H_7 + OH \quad (30)$$

The rate coefficient for reaction 30 has been studied very well, as reviewed by Tsang.[23] Here, note that reaction path degeneracy, $l^\ddagger$, is different for reaction 1a and for reaction 30, i.e., $l^\ddagger(1a) = 1$ and $l^\ddagger(30) = 2$. So a half-value of k_{30} is shown with the broken line in Figure 5. The present result of k_{1a} is found to be much smaller than $k_{30}/2$, suggesting that the C−H bond strength in CF_3CHFCF_3 molecules is enhanced by an electron-attracting effect of the surrounding fluorine atoms. The G2-(MP2) ab initio calculation also supports this suggestion: the energy barrier of reaction 1a is 56 kJ mol^{-1}, whereas that of reaction 30 is only 23 kJ mol^{-1}.

Reaction of CF_3CHFCF_3 with H. Figure 6 shows the energy diagram for the following competing channels in the reaction of CF_3CHFCF_3 with H:

$$CF_3CHFCF_3 + H \rightarrow i\text{-}C_3F_7 + H_2 \quad (2a)$$

$$CF_3CHFCF_3 + H \rightarrow i\text{-}C_3HF_6 + HF \quad (2b)$$

$$CF_3CHFCF_3 + H \rightarrow n\text{-}C_3HF_6 + HF \quad (2c)$$

The energy barriers of reactions 2b and 2c are 80 and 118 kJ mol^{-1} higher than that of reaction 2a, although the enthalpies of the F abstractions are smaller than that of the H abstraction. These differences in energy barrier mean that the branching ratios, k_{2b}/k_{2a} and k_{2c}/k_{2a}, can be estimated to be 1×10^{-4} and 2×10^{-6} at 1100 K, assuming that their preexponential factors are identical. So we can conclude that reaction 2a is the dominant channel, and that reactions 2b and 2c are negligible.

To research the kinetics of reaction 2a, we measured H atom decay in mixtures of 0.05−0.1% CF_3CHFCF_3 and 2−4 ppm C_2H_5I diluted in argon. Figure 7 shows typical concentration profiles of H atoms in the C_2H_5I/Ar mixtures with and without CF_3CHFCF_3. In the C_2H_5I/Ar mixture, H atoms are immediately produced through a series of reactions 18a and −19 and then the concentration reaches a nearly constant value.

$$C_2H_5I \rightarrow C_2H_5 + I \quad (18a)$$

$$C_2H_5(+M) \rightarrow C_2H_4 + H(+M) \quad (-19)$$

At temperatures lower than 1000 K, this initial formation of H atoms was not enough to research the kinetics, so that all of the experiments for the reaction CF_3CHFCF_3 + H were performed over 1000 K. On the other hand, in the presence of CF_3CHFCF_3, H atoms are gradually reduced through reaction 2a after the initial production.

To determine k_{2a}, the concentration profiles of H atoms were calculated by numerically integrating the rate equations in scheme II of Table 1. Time-resolved profiles of the normalized first-order sensitivity coefficients for H atom concentration, $\partial(\log [H])/(\partial \log k_j)$, are shown in Figure 8. The analysis shows that the concentration of H atoms is greatly influenced by reaction 18a at the early reaction time and by reaction 2a at the later time, and that the contribution of the other reactions is negligible. Because the time range when reaction 2a has an influence on the H atom concentration is different from that of reaction 18a, the rate coefficients, k_{18a} and k_{2a}, were simultaneously optimized by fitting the calculated profiles to the observed ones, as shown in Figure 7.

The values of k_{18a} determined in this procedure are plotted in Figure 9. The present results are in excellent agreement with our colleague's previous data,[20] which have been obtained directly by monitoring H and I atoms behind shock waves. This confirms that the simultaneous determination of k_{18a} and k_{2a} is essentially correct. An Arrhenius plot of k_{2a} is shown in Figure 10. These numerical data are summarized in the Supporting Information, together with the detailed experimental conditions. The measured values of k_{2a} have no dependence on the initial concentration of CF_3CHFCF_3. A least-squares fit of the data yielded the following Arrhenius expression over the temperature range of 1000 to 1180 K:

$$k_{2a} = 10^{-9.15\pm0.66} \times \exp[-(63 \pm 14)\ \text{kJ mol}^{-1}/RT]\ \text{cm}^3\ \text{molecule}^{-1}\ \text{s}^{-1}$$

The present result of k_{2a} is much smaller than the half-value of the rate coefficient for the reaction $C_3H_8 + H \rightarrow i\text{-}C_3H_7 + H_2$ (31),[23] similarly to the reactions with $O(^3P)$ atoms.

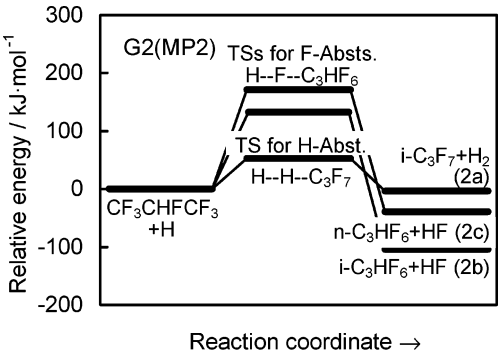

Figure 6. Energy diagram for the reaction CF_3CHFCF_3 + H. The energies are calculated at the G2(MP2) level and are corrected for the zero-point vibrations.

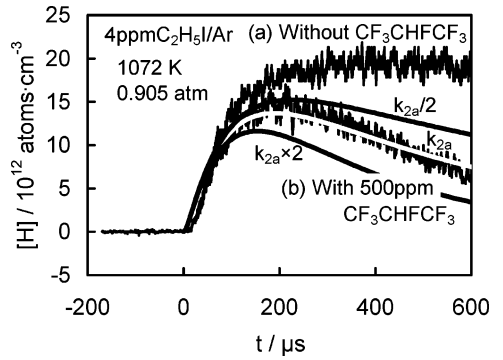

Figure 7. Typical concentration profiles of H atoms in (a) 4 ppm C_2H_5I/Ar and (b) 500 ppm CF_3CHFCF_3/4 ppm C_2H_5I/Ar mixtures. The white and the two black lines denote profiles calculated by varying the rate coefficient for reaction 2a in scheme II of Table 1.

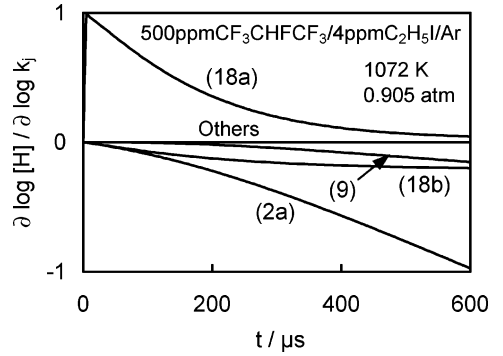

Figure 8. Sensitivity analysis of the rate coefficients for H atom concentration in 500 ppm CF_3CHFCF_3/4 ppm C_2H_5I/Ar mixture. Numbers in the figure denote the reaction numbers defined in Table 1.

The measured k_{2a} is larger than k_{1a} by a factor of 7−8 over the present experimental temperature range. Generally, the relationship of the rate coefficients between the reactions of fluorine-free alkanes, C_nH_{2n+2}, with $O(^3P)$ and H atoms is either $k(C_nH_{2n+2}+O) > k(C_nH_{2n+2}+H)$ or $k(C_nH_{2n+2}+O) \approx k(C_nH_{2n+2}+H)$, contrary to the order of the reactions of CF_3CHFCF_3. This disagreement seems to be caused by the following reason: the electronic density around a hydrogen atom abstracted from CF_3CHFCF_3 is much lower than that from C_nH_{2n+2}, due to an electron-attracting effect of the surrounding fluorine atoms. When such electron-attracting groups exist in the molecules, the reaction with $O(^3P)$ atoms is deactivated more than that with H atoms, because $O(^3P)$ atoms act as a strong electrophilic reagent. The G2(MP2) ab initio calculation also supports this consideration: the energy barriers of reactions 1a and 2a are 56 and 53 kJ mol^{-1}, whereas those of reactions 30 and 31 are 23 and 37 kJ mol^{-1}.

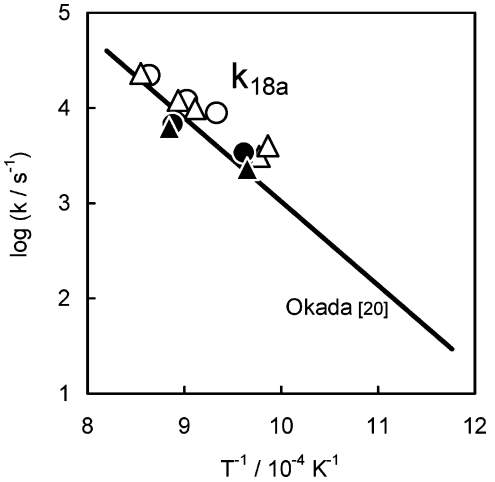

Figure 9. Arrhenius plot of the rate coefficient for reaction 18a: (●) 500 ppm CF_3CHFCF_3/2 ppm C_2H_5I/Ar; (▲) 0.1% CF_3CHFCF_3/2 ppm C_2H_5I/Ar; (○) 500 ppm CF_3CHFCF_3/4 ppm C_2H_5I/Ar; (△) 0.1% CF_3CHFCF_3/4 ppm C_2H_5I/Ar. The solid line denotes the previous data reported by Okada.[20]

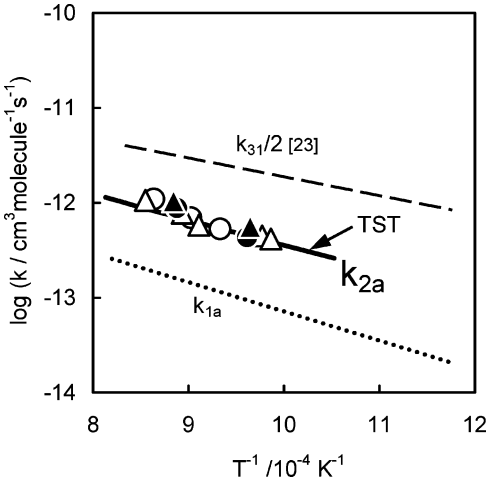

Figure 10. Arrhenius plot of the rate coefficient for reaction 2a. Symbols mean the mixtures with the same compositions as those in Figure 9. The rate coefficient for reactions 1a is also described with the dotted lines to compare with k_{2a}. The broken line denotes half of the reaction $C_3H_8 + H \rightarrow i\text{-}C_3H_7 + H_2$ (31).[23] The solid line shows the TST result calculated with $E_0^{\ddagger}(2a) = 41$ kJ mol^{-1}.

TST Calculation. To evaluate the validity of the experimental results, the rate coefficients k_{1a} and k_{2a} were calculated with the transition-state theory (TST). The TST rate coefficient can be expressed as follows:

$$k^{\mathrm{TST}}_{\mathrm{CF_3CHFCF_3+X}} = \Gamma l^{\ddagger}\frac{k_B T}{h}\frac{Q^{\ddagger}}{Q_{\mathrm{CF_3CHFCF_3}}Q_{\mathrm{X}}} \times \exp\left[-\frac{E_0^{\ddagger}(\mathrm{CF_3CHFCF_3+X})}{RT}\right]$$

where Γ is a correction factor for quantum mechanical tunneling, $l^{\ddagger}$ is the reaction path degeneracy, $E_0^{\ddagger}$ is the energy barrier at 0 K, and $Q^{\ddagger}$ and Q_R (R: CF_3CHFCF_3 and X) are the partition functions of the transition state and the reactants, respectively. k_B and h are the Boltzmann and Planck constants. All parameters required for the TST calculation are summarized in Table 2. The geometries of the transition states and the reactants, which are necessary to get the moments of inertia, were taken from the results of an ab initio MO calculation at the MP2(full)/6-31G(d) level. The vibrational frequencies were computed at the HF/6-31G(d) level and scaled by a factor of 0.8929[24] to compensate for known systematic errors. All internal rotations were treated as free rotors. The parameter Γ was roughly estimated by using the Wigner expression[25] based on the imaginary frequency for motion along the reaction coordinate, ν_i, because the tunneling effect was not large under the present conditions.

$$\Gamma \approx 1 - \frac{1}{24}\left(\frac{h\nu_i}{k_B T}\right)^2\left(1 + \frac{k_B T}{E_0^{\ddagger}}\right)$$

The energy barrier, $E_0^{\ddagger}$, which is the most sensitive parameter in the calculation, was adjusted until the TST rate coefficient most closely matched the present experimental results. The TST results obtained in this way are shown with the solid lines in Figures 5 and 10. The fittings yielded $E_0^{\ddagger}(1a) = 51$ kJ mol^{-1} and $E_0^{\ddagger}(2a) = 41$ kJ mol^{-1}. These values are somewhat smaller than the energy barriers calculated at G2(MP2) but are within the expected uncertainty of the calculated energies:[14] (56 ± 13) and (53 ± 13) kJ mol^{-1} for reactions 1a and 2a. So the experimentally determined rate coefficients were confirmed to be theoretically acceptable.

Reactions of $CHF_2CF_2CF_3$ with $O(^3P)$ and H. Straight-chain heptafluoropropanes have two structural isomers depending on the location of a hydrogen atom: CF_3CHFCF_3 and $CHF_2CF_2CF_3$. To compare the reactivities between these isomers, we determined the rate coefficients for the reactions $CHF_2CF_2CF_3 + O(^3P) \rightarrow n\text{-}C_3F_7 + OH$ (3a) and $CHF_2CF_2CF_3 + H \rightarrow n\text{-}C_3F_7 + H_2$ (4a) experimentally by using the same technique. The measured values of k_{3a} and k_{4a} are plotted in Figure 11, together with k_{1a} and k_{2a}. These numerical data can be found in the Supporting Information. The Arrhenius expressions were obtained by least-squares fits as follows:

$$k_{3a} = 10^{-10.13\pm0.52} \times \exp[-(55 \pm 10)\ \mathrm{kJ\ mol^{-1}}/RT]\ \mathrm{cm^3\ molecule^{-1}\ s^{-1}} \quad (880-1180\ \mathrm{K})$$

$$k_{4a} = 10^{-9.44\pm0.32} \times \exp[-(57 \pm 7)\ \mathrm{kJ\ mol^{-1}}/RT]\ \mathrm{cm^3\ molecule^{-1}\ s^{-1}} \quad (1000-1180\ \mathrm{K})$$

Figure 11 shows that the absolute values of k_{3a} are approximately 50% larger than those of k_{1a}, whereas k_{4a} has the same values as k_{2a}.

To discuss this difference in reactivities, we calculated the energy barriers of reactions 1a−4a at the G2(MP2) level. The results are summarized in Table 3. 1*H*-Heptafluoropropanes have two conformers: hydrogen atoms are located in (α) and out (β) of the C−C−C plane. The energy gap between conformers α and β is only 1.0 kJ mol^{-1} ($E(\alpha) > E(\beta)$), and the energy barrier of a transition from α to β is 11.7 kJ mol^{-1}. This means that both conformers can freely be changed to each other in the present temperature range. Table 3 shows that reactions 3a and 4a proceed via conformer α, because the energy barriers of the reactions of conformer α with $O(^3P)$ and H atoms are ≈3.0 kJ mol^{-1} lower than those of conformer β. The differences in calculated energy barriers are 6.2 kJ mol^{-1} between reactions 1a and 3a but only 1.8 kJ mol^{-1} between reactions 2a and 4a, resulting in the relationships of $k_{3a} \approx 1.5k_{1a}$ and $k_{4a} \approx k_{2a}$.

Such a large difference in energy barriers between reactions 1a and 3a can be explained as follows: as mentioned in the above subsection, the reactivity with $O(^3P)$ atoms is dependent

TABLE 2: TST Parameters for the Reactions $CF_3CHFCF_3 + O(^3P) \rightarrow CF_3CFCF_3 + OH$ (1a) and $CF_3CHFCF_3 + H \rightarrow CF_3CFCF_3 + H_2$ (2a)

	reactant			transition state	
	CF_3CHFCF_3	$O(^3P)$	H	TS (1a)	TS (2a)
molecular weight, g mol^{-1}	170.030	15.999	1.008	186.029	171.038
spin multiplicity	singlet	triplet	doublet	triplet	doublet
$E_0^{\ddagger}$, kJ mol^{-1}				adjusted	adjusted
$I^{\ddagger}$				1	1
freedom of external rotations	3	0	0	3	3
I_a, g cm^2	4.034×10^{-38}			6.241×10^{-38}	4.199×10^{-38}
I_b, g cm^2	7.853×10^{-38}			8.951×10^{-38}	8.104×10^{-38}
I_c, g cm^2	8.928×10^{-38}			1.022×10^{-37}	9.032×10^{-38}
freedom of internal rotations	2	0	0	2	2
I_{r1}, g cm^2	1.149×10^{-38}			1.209×10^{-38}	1.143×10^{-38}
I_{r2}, g cm^2	1.149×10^{-38}			1.209×10^{-38}	1.143×10^{-38}
vibrational frequencies, cm^{-1}	2966			2810i[a]	2178i[a]
	1428			1356	1386
	1392			1351	1369
	1324			1292	1345
	1296			1274	1286
	1280			1254	1264
	1242			1231	1242
	1224			1189	1227
	1150			1040	1191
	1131			928	1135
	896			905	1127
	853			873	935
	725			740	789
	669			680	706
	593			595	681
	535			537	598
	519			520	541
	502			517	520
	442			444	500
	335			335	445
	314			330	337
	283			309	315
	231			286	310
	214			235	283
	152			197	270
				149	231
				91	196
				72	146

[a] Imaginary frequencies with the reaction coordinates.

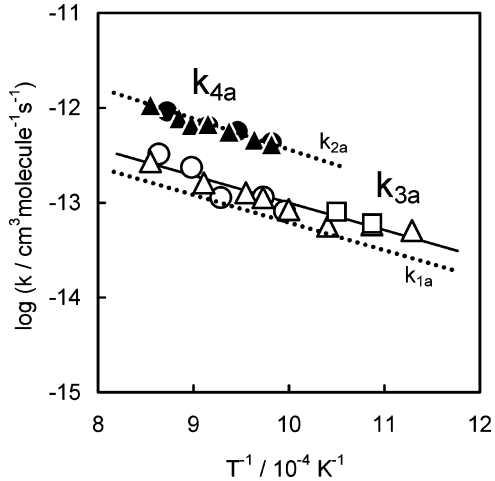

Figure 11. Arrhenius plots of the rate coefficients for reactions 3a and 4a: (○) 0.1% $CHF_2CF_2CF_3$/200 ppm SO_2/Ar, ArF-LP; (□) 0.2% $CHF_2CF_2CF_3$/200 ppm SO_2/Ar, ArF-LP; (△) 0.3% $CHF_2CF_2CF_3$/200 ppm SO_2/Ar, ArF-LP for k_{3a}. (●) 500 ppm $CHF_2CF_2CF_3$/4 ppm C_2H_5I/Ar; (▲) 0.1% $CHF_2CF_2CF_3$/4 ppm C_2H_5I/Ar for k_{4a}. The rate coefficients for reactions 1a and 2a are also described with the dotted lines to compare with k_{3a} and k_{4a}.

on the electronic density around atoms or functional groups attacked by $O(^3P)$ atoms, because $O(^3P)$ atoms act as a strong electrophilic reagent. Mulliken's population analysis shows that the electronic charge of a hydrogen atom in CF_3CHFCF_3 takes a bigger positive value than that in $CHF_2CF_2CF_3$, leading to $E(1a) > E(3a)$, i.e., $k_{3a} > k_{1a}$. This feature can also be found for the reactions of propane with $O(^3P)$ atoms; the abstraction of primary H atoms occurs more easily than that of secondary H atoms.[23]

TABLE 3: Energy Barriers Calculated at the G2(MP2) Level for the Reactions of 1*H*- and 2*H*-Heptafluoropropanes with $O(^3P)$ and H Atoms[a]

		$CHF_2CF_2CF_3$	
reactant	CF_3CHFCF_3	conformer α[b]	conformer β[b]
$O(^3P)$	56.4	50.2	52.7
H	52.5	50.7	53.7

[a] Energy barriers in kJ mol^{-1}. [b] Conformers α and β mean that hydrogen atoms are located in and out of the C−C−C plane, respectively.

Conclusions

The rate coefficients for the reactions of 2*H*-heptafluoropropane with $O(^3P)$ and H atoms were experimentally determined first by the present work. These results showed that reaction 2a was faster than reaction 1a by a factor of 7−8, contrary to the reactions of fluorine-free alkanes with $O(^3P)$ and H atoms. Both k_{1a} and k_{2a} were much smaller than the previous kinetic data for the analogous reactions of propane, demonstrating that the C−H bond strength in CF_3CHFCF_3 molecules was enhanced by an electron-attracting effect of the surrounding fluorine

atoms. The TST calculation proved that the present experimental results were theoretically valid.

The reaction mechanism for CF_3CHFCF_3 has previously been reported by only two research groups,[7,8] but most of the kinetic data for the elementary steps of C3 fluorocarbons, containing reactions 1a and 2a, are estimated from those for the analogous reactions of C2 fluorocarbons or fluorine-free hydrocarbons. The values of k_{1a} estimated by Hynes et al.[8] are on average 3-fold larger than the present data, whereas their k_{2a} is only one-fiftieth of ours. So, we investigated how much these big differences affected the results of the numerical simulation for CF_3CHFCF_3-inhibited flames. The model calculation was carried out for freely propagating steady laminar one-dimensional premixed flames by using the Sandia PREMIX program code.[26] The reaction mechanism used was composed of three distinct submechanisms: GRI-Mech[27] for hydrogen and hydrocarbon oxidation (36 species and 194 reactions), a comprehensive C1 and C2 hydrofluorocarbon mechanism[6] (51 species and 585 reactions), and the CF_3CHFCF_3 oxidation mechanism published by Hynes et al.[8] (9 species and 42 reactions). The burning velocity of an uninhibited flame formed in a mixture of 9.5% CH_4 and 19.0% O_2 diluted in N_2 was calculated to be 37.7 cm s^{-1} at atmospheric pressure. On the other hand, the burning velocity of a flame inhibited with 0.5% CF_3CHFCF_3 was 31.9 cm s^{-1} when the present data for k_{1a} and k_{2a} were used. This is exactly the same value as the velocity calculated using Hynes' original kinetic data for k_{1a} and k_{2a}, demonstrating that the modifications of k_{1a} and k_{2a} give no effect on the burning velocity. However, a total flux analysis, which integrates each reaction rate along the flow line from $x = -\infty$ to $+\infty$, showed that the reaction pathway for the consumption of CF_3CHFCF_3 demonstrated a big difference due to the modifications of k_{1a} and k_{2a}. In the reaction model before the modifications, only the thermal decomposition reactions 7a and 7b can be regarded as main channels of the CF_3CHFCF_3 consumption, and their contribution ratios are 0.46 and 0.47. In the revised reaction model, the rate of reaction 2a becomes larger, and reactions 2a, 7a, and 7b contribute with ratios of 0.38, 0.28, and 0.30, respectively. This means that not only C_3F_6 and CF_3CHF but also CF_3CFCF_3 is very important as a major product of the CF_3CHFCF_3 consumption, and that subsequent reactions of these species need to be studied to construct a comprehensive reaction mechanism for the CF_3CHFCF_3 combustion. The kinetics of the reactions of CF_3CFCF_3 radicals, which has never previously been researched at any temperatures, will be clarified in our next paper.

Acknowledgment. We express our gratitude to Prof. Frank Scott Howell, S. J., for his valuable comments.

Supporting Information Available: Tables of the kinetic data measured for the reactions of CF_3CHFCF_3 and $CHF_2CF_2CF_3$ with $O(^3P)$ and H atoms, together with the detailed experimental conditions. This material is available free of charge via the Internet at http://pubs.acs.org.

References and Notes

(1) Robin, M. L. In *Halon Replacements*; Miziolek, A. W., Ysang, W., Eds.; American Chemical Society: Washington, DC, 1995; p 85.

(2) Rosser, W. A.; Wise, H.; Miller, J. *Seventh Symposium (International) on Combustion*; The Combustion Institute: Pittsburgh, PA, 1959; p 175.

(3) Biordi, J. C.; Lazzara, C. P.; Papp, J. F. *J. Phys. Chem.* **1978**, *82*, 125.

(4) Westbrook, C. K. *Combust. Sci. Technol.* **1983**, *34*, 201.

(5) Molina, M. J.; Rowland, F. S. *Nature* **1974**, *249*, 810.

(6) Burgess, D. R. F, Jr.; Zachariah, M.; Tsang, W.; Westmoreland, P. R. *Prog. Energy Combust. Sci.* **1995**, *21*, 453.

(7) Sanogo, O.; Delfau, J.-L.; Akrich, R.; Vovelle, C. *Combust. Sci. Technol.* **1997**, *122*, 33.

(8) Hynes, R. G.; Mackie, J. C.; Masri, A. R. *Combust. Flame* **1998**, *113*, 554.

(9) Takahashi, K.; Yamamori, Y.; Inomata T. *J. Phys. Chem. A* **1997**, *101*, 9105.

(10) Takahashi, K.; Sekiuji, Y.; Yamamori, Y.; Inomata T.; Yokoyama, K. *J. Phys. Chem. A* **1998**, *102*, 8339.

(11) Yamamori, Y.; Takahashi, K.; Inomata T. *J. Phys. Chem. A* **1999**, *103*, 8803.

(12) Hynes, R. G.; Mackie, J. C.; Masri, A. R. *J. Phys. Chem. A* **1999**, *103*, 54.

(13) Frisch, M. J.; Trucks, G. W.; Schlegel, H. B.; Scuseria, G. E.; Robb, M. A.; Cheeseman, J. R.; Zakrzewski, V. G.; Montgomery, J. A., Jr.; Stratmann, R. E.; Burant, J. C.; Dapprich, S.; Millam, J. M.; Daniels, A. D.; Kudin, K. N.; Strain, M. C.; Farkas, O.; Tomasi, J.; Barone, V.; Cossi, M.; Cammi, R.; Mennucci, B.; Pomelli, C.; Adamo, C.; Clifford, S.; Ochterski, J.; Petersson, G. A.; Ayala, P. Y.; Cui, Q.; Morokuma, K.; Rega, N.; Salvador, P.; Dannenberg, J. J.; Malick, D. K.; Rabuck, A. D.; Raghavachari, K.; Foresman, J. B.; Cioslowski, J.; Ortiz, J. V.; Baboul, A. G.; Stefanov, B. B.; Liu, G.; Liashenko, A.; Piskorz, P.; Komaromi, I.; Gomperts, R.; Martin, R. L.; Fox, D. J.; Keith, T.; Al-Laham, M. A.; Peng, C. Y.; Nanayakkara, A.; Challacombe, M.; Gill, P. M. W.; Johnson, B.; Chen, W.; Wong, M. W.; Andres, J. L.; Gonzalez, C.; Head-Gordon, M.; Replogle, E. S.; Pople, J. A. *Gaussian 98*, Revision A.11.3; Gaussian, Inc.: Pittsburgh, PA, 2002.

(14) Curtiss, L. A.; Raghavachari, K.; Pople, J. A. *J. Chem. Phys.* **1993**, *98*, 1293.

(15) Kee, R. J.; Rupley, F. M.; Miller, J. A. *Chemkin-II: A Fortran Chemical Kinetics Package for the Analysis of Gas-Phase Chemical Kinetics*; Sandia National Laboratories Report SAND89-8009; Sandia Laboratories: Albuquerque, NM, 1993.

(16) Lutz, A. E.; Kee, R. J.; Miller, J. A. *SENKIN: A Fortran Program for Predicting Homogeneous Gas Phase Chemical Kinetics with Sensitivity Analysis*; Sandia National Laboratories Report SAND87-8248; Sandia Laboratories: Albuquerque, NM, 1991.

(17) Just, Th.; Rimpel, G. *Eleventh Symposium (International) on Shock Tubes and Waves*; Springer-Verlag: Berlin, 1978; p 226.

(18) Singleton, D. L.; Cvetanovic, R. J. *J. Phys. Chem. Ref. Data* **1988**, *17*, 1377.

(19) Baulch, D. L.; Drysdale, D. D.; Duxbury, J.; Grant, S. J. *Evaluated Kinetic Data for High Temperature Reactions. Volume 3 Homogeneous Gas Phase Reactions of the O_2-O_3 System, the CO−O_2-H_2 System, and of Sulphur-containing Species*; Butterworths: London, 1976; p 33.

(20) Okada, K. M.S. Thesis; Sophia University, 1996.

(21) Miller, J. A.; Bowman, C. T. *Prog. Energy Combust. Sci.* **1989**, *15*, 287.

(22) Westbrook, C. K., *Nineteenth Symposium (International) on Combustion*; The Combustion Institute: Pittsburgh, PA, 1982; p 127.

(23) Tsang, W. *J. Phys. Chem. Ref. Data* **1988**, *17*, 87.

(24) Foresman, J. B.; Frisch, M. J. *Exploring Chemistry with Electronic Structure Methods*, 2nd ed.; Gaussian, Inc.: Pittsburgh, PA, 1996; p 64.

(25) Shavitt, I. *J. Chem. Phys.* **1959**, *31*, 1359.

(26) Kee, R. J.; Grcar, J. F.; Smooke, M. D.; Miller, J. A. *A Fortran Program for Modeling Steady Laminar One-Dimensional Premixed Flames*; Sandia National Laboratories Report SAND85-8240; Sandia Laboratories: Albuquerque, NM, 1985.

(27) Smith, G. P.; Golden, D. M.; Frenklach, M.; Moriarty, N. W.; Eiteneer, B.; Goldenberg, M.; Bowman, C. T.; Hanson, R. K.; Song, S.; Gardiner, W. C., Jr.; Lissianski, V. V.; Qin, Z. *GRI-Mech 3.0*; http://www.me.berkekey.edu/gri_mech/, 1999.